HHS Public Access

Author manuscript

J Comp Neurol. Author manuscript; available in PMC 2019 August 15.

Published in final edited form as:

J Comp Neurol. 2018 August 15; 526(12): 1896–1909. doi:10.1002/cne.24456.

Cone synapses in mammalian retinal rod bipolar cells

Ji-Jie Pang, **Zhuo Yang**, **Roy A. Jacoby**, and **Samuel M. Wu**

Abstract

Some mammalian rod bipolar cells (RBCs) can receive excitatory chemical synaptic inputs from both rods and cones (DBC_{R2}), but anatomical evidence for mammalian cone-RBC contacts has been sparse. We examined anatomical cone-RBC contacts using neurobiotin (NB) to visualize individual mouse cones and standard immuno-markers to identify RBCs, cone pedicles and synapses in mouse and baboon retinas. Peanut agglutinin (PNA) stained the basal membrane of all cone pedicles, and mouse cones were positive for red/green (R/G)-opsin, whereas baboon cones were positive for calbindin D-28k. All synapses in the outer plexiform layer were labeled for synaptic vesicle protein 2 (SV2) and PSD (postsynaptic density)-95, and those that coincided with PNA resided closest to bipolar cell somas. Cone-RBC synaptic contacts were identified by: 1) RBC dendrites deeply invaginating into the center of cone pedicles (invaginating synapses), 2) RBC dendritic spines intruding into the surface of cone pedicles (superficial synapses), and 3) PKCα immunoreactivity coinciding with synaptic marker SV2, PSD-95, mGluR6, G protein beta 5 or PNA at cone pedicles. One RBC could form 0–1 invaginating and 1–3 superficial contacts with cones. 20.7% and 38.9% of mouse RBCs contacted cones in the peripheral and central retina ($p<0.05$, n=14 samples), respectively, while 34.4% (peripheral) and 48.5% (central) of cones contacted RBCs ($p>0.05$). In baboon retinas (n=4 samples), cone-RBC contacts involved 12.2% of RBCs (n=416 cells) and 22.5% of cones (n=225 cells). This suggests that rod and cone signals in the ON pathway are integrated in some RBCs before reaching AII amacrine cells.

Graphical Abstract

Correspondence to: Ji-Jie Pang, M.D., Ph.D., Department of Ophthalmology, Baylor College of Medicine, One Baylor Plaza, NC 205, Houston, Texas 77030, Tel: (713) 798 4349; Fax: (713) 798 4364; jpang@bcm.edu.

Conflict of interest statement

All authors do not have any known or potential conflict of interest including financial, personal or other relationships with other people or organizations within three years of beginning the submitted work that could inappropriately influence, or be perceived to influence, their work.

Data Accessibility

All data related is included in this manuscript.

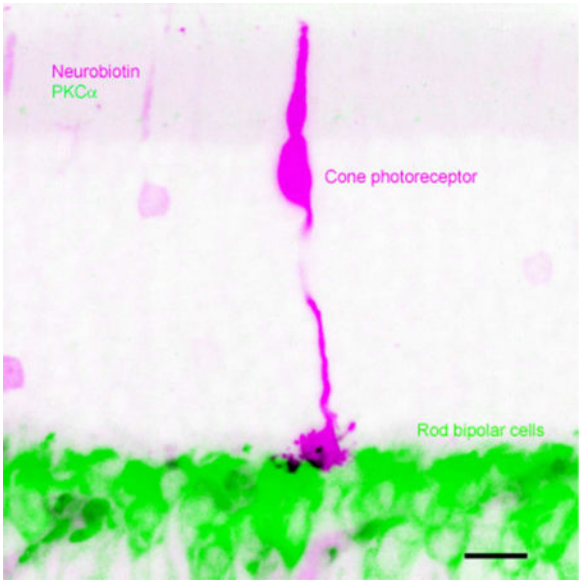

Using confocal microscopy combined with cellular and synaptic markers, the authors show that a subset of mouse and primate rod bipolar cells receives synapses from both cone and rod photoreceptors. These synapses allow such a novel subtype of rod bipolar cells to integrate rod and cone signals for better processing of mesopic light signals in the retinal ON pathway.

Keywords

Rod bipolar cell; Mouse; Primate; Cone synapse; Tracer injection; Confocal microscopy; Immunohistology; Synaptic vesicle protein RRID:AB_2315387; Postsynaptic density-95 RRID: AB_10807979; PKCα RRID: AB_477345; RRID: AB_2313718; mGluR6 RRID: AB_784501; RRID: AB_2650488

Introduction

Rod and cone pathways are fundamental light signaling circuitries in the retina. Recently, a subset of mammalian rod bipolar cells (RBCs), which had been long thought to exclusively serve the rod pathway, has been suggested to receive excitatory chemical synaptic inputs from both rod and cone photoreceptors (Pang et al., 2010). These bipolar cells were physiologically identified as rod and cone-driven depolarizing bipolar cells (DBCs) but exhibited RBC morphology and PKCα immunoreactivity, thus, they were named DBC_{R2}. Observation of mixed rod-cone inputs in RBCs in mammalian retina was surprising but not fully unexpected after mammalian OFF BCs, once thought to be purely cone-driven cells, had been found to receive rod chemical synaptic inputs. Rod signals may drive cone OFF BCs via chemical synapses, known as the tertiary rod signaling pathway in the mammalian retina, and this has been demonstrated by electrophysiological studies in the ground squirrel and mouse retina (Li, Chen, & DeVries, 2010; Pang, Gao, Paul, & Wu, 2012; Soucy, Wang, Nirenberg, Nathans, & Meister, 1998) and from electron microscopic studies in the retinas of mice, rats, rabbits, and cats (Soucy et al., 1998; Hack, Peichl, & Brandstatter, 1999; Tsukamoto, Morigiwa, Ueda, & Sterling, 2001; Fyk-Kolodziej, Qin, & Pourcho, 2003; Li,

Keung, & Massey, 2004). However, anatomical evidence for mammalian cone-RBC synaptic contacts has been sparse.

BCs are retinal interneurons, which receive glutamatergic synapses from rod and cone photoreceptors and output signals to the inner retina. There are about 11–13 subtypes of mammalian BCs that primarily receive cone inputs (Dowling, 2012; Masland, 2012; Euler, Haverkamp, Schubert, & Baden, 2014; Joo, Peterson, Haun, & Dacey, 2011; Puthussery, Venkataramani, Gayet-Primo, Smith, & Taylor, 2013; Puthussery et al., 2014), while only a single *morphological* type of RBC has been found in all mammalian retinas (Grunert & Martin, 1991; Greferath, Grunert, & Wassle, 1990; Kolb, Zhang, & Dekorver, 1993). Each RBC collects input from between 15 and 30 rod spherules in the OPL (Greferath et al., 1990; Kolb et al., 1993). RBCs in primate (Grunert & Martin, 1991) and rabbit retinas (Dacheux & Raviola, 1986) primarily contact rods, but occasionally they also contact cones. Cone-RBC synapses have been recently reported in the mouse retina (Behrens, Schubert, Haverkamp, Euler, & Berens, 2016). Nocturnal animals, such as most rodents, use rod vision more intensively than cone vision compared with diurnal animals. Yet, the population of rod-cone-driven RBCs in other mammals has not been reported, and whether this RBC population differs among mammals is not clear. The significance of the presumably rare cone-RBC synapses in mammalian night (scotopic) vision and mesopic vision is uncertain.

Electron microscopic investigation of Golgi-impregnated RBCs first showed that RBC dendrites penetrate into the rod spherule to make an invaginating ribbon-related type of contact (Kolb, 1970). Usually two to four RBC processes invaginate each rod spherule (Grunert & Martin, 1991). RBCs in most mammalian retinas abundantly express protein kinase C alpha (PKCα), which allows reliable identification of RBCs under the light and fluorescent microscopes (Greferath et al., 1990; Kolb et al., 1993; Wassle, Puller, Muller, & Haverkamp, 2009). PKCα is a serine/threonine protein kinase that undergoes calcium dependent translocation from the cytosol to the plasma membrane, where it is activated upon binding to diacylglycerol (DAG) (Wu-Zhang & Newton, 2013). PKCα modulates amplitude and kinetics of RBC light responses (Xiong et al., 2015), but its mechanism is not completely clear. Typical mammalian RBCs often show a long thin axon and narrow-field axonal terminal, appearing as a few irregular globules in living retinas (Pang, Gao, & Wu, 2004) or clumpy processes in fixed tissues (Greferath et al., 1990; Kolb et al., 1993) around the proximal border of the inner plexiform layer (IPL). Under an electron microscope, RBC axonal terminals may be identified as the largest neuronal processes in the IPL with rich synaptic vesicles, ribbon synapses and originated from a cell that receive synapses predominantly from rods (Grunert & Martin, 1991; Strettoi, Dacheux, & Raviola, 1990; Kolb, 1970). PKCα labeling is not ideal for electron microscopy, because the labeling does not tolerate glutaraldehyde concentration above 0.1%, which is, on the other hand, required for better preserving the ultrastructure (Grunert & Martin, 1991). But PKCα-labeled samples were still good enough for some studies to reveal rod-RBC synapses, as well as occasional cone-RBC synapses (Grunert & Martin, 1991; Dacheux & Raviola, 1986), at the ultrastructural level.

Photoreceptor-BC synapses are glutamatergic chemical synapses. Synaptic vesicle protein 2 (SV2) is a membrane glycoprotein and a synaptic vesicle-specific transporter (Bajjalieh,

Peterson, Shinghal, & Scheller, 1992; Feany, Lee, Edwards, & Buckley, 1992), thus, it has been widely used to study synaptic contacts in the retina (Wang, Janz, Belizaire, Frishman, & Sherry, 2003; O'Brien, Nguyen, & Mills, 2004), including rod and cone synapses. Another well-studied synaptic marker is PSD-95 (Koulen, Fletcher, Craven, Bredt, & Wassle, 1998; El-Husseini, Schnell, Chetkovich, Nicoll, & Bredt, 2000). PSD-95 is a guanylate kinase and a major scaffolding protein in the excitatory postsynaptic density. In the retina, PSD-95 is most prominently expressed in the outer plexiform layer (OPL), particularly in axon terminals of rods and cones, rod spherules and cone pedicles (Koulen et al., 1998; Aartsen et al., 2006). Electron microscopic studies showed that PSD-95 localized presynaptically within the photoreceptor terminals (Koulen et al., 1998). From a variety of species, including the fish, rabbit, monkey, human and chick, PNA has been showed to locate exclusively in cone photoreceptors and associate with the large synaptic pedicles of cones (Blanks & Johnson, 1984; Wassle et al., 2009). Glutamate hyperpolarizes ON bipolar cells (including RBCs) by binding to the metabotropic glutamate receptor mGluR6, and guanine nucleotide-binding proteins subunit beta 5 has been found to precisely co-localize with mGluR6 (Mojumder, Qian, & Wensel, 2009; Morgans et al., 2007). Using confocal microscopy and individual cone labeling, along with above-mentioned standard RBC, cone and synaptic markers, this study examined cone-RBC synapses in the mouse and baboon retinas. Our data showed that mouse and primate retinas both possessed cone-RBC synapses, while rodent RBCs contact cones more frequently.

Materials and Methods

Animals

The mice used in this study were C57BL/6J mice purchased from Jackson Laboratory (Bar Harbor, ME) and mGluR6 knockout mice obtained from Dr. David Copenhagen (University of California, San Francisco) with permission from Dr Nakanishi, which was previously described (Masu et al., 1995). The mice were 2 – 8-month-old males and females. All procedures used in this study followed the NIH animal care guidelines and ARVO Statement for the Use of Animals in Ophthalmic and Vision Research, as well as the relevant requirements of the Baylor College of Medicine Animal Care and Use Committee. Mice were anesthetized with an intraperitoneal injection of ketamine (200 mg/kg) and xylazine (10 mg/kg). The eyes were enucleated after the animals were deeply anesthetized and decapitated. Retinas were immediately dissected in oxygenated Ames medium in room temperature (Pang, Paul, & Wu, 2013; Pang, Gao, & Wu, 2010). Baboon (*Papio cynocephalus anubis*) eyes were enucleated within 10 minutes after the animal had been overdosed with sodium pentobarbital (50–100 mg/kg, IV) by other investigators at the conclusion of experiments that did not involve the eyes. The eyes were hemisected and the eyecups with attached retinas were incubated in room temperature in oxygenated Ames medium for 3–5 hours before dissecting retinas (Jacoby, Stafford, Kouyama, & Marshak, 1996). Data on the baboon retina were obtained from the para-central (3–7 mm away from the fovea) and peripheral retina (> 7 mm away from the fovea). All isolated retinas were fixed with 4% of paraformaldehyde in phosphate buffer (pH 7.4) for 1–2 hours in 4°C. Other procedures followed previously established protocol (Pang et al., 2013; Pang et al., 2010).

Antibody characterization

The anti-PKCα antibody from Sigma has been tested in immunoblotting in rat brain extract, and it recognized a heavy band at ~ 76 kDa and a very weak band at 40 kDa, while the predicted molecular weight of the PKCα was 76–93 kDa. The staining was specifically inhibited by PKCα immunizing peptide (659–672). The monoclonal anti-PKCα antibody from BD transduction identified a single band at 82 kDa from a rat cerebrum lysate. Labeling patterns of these antibodies in current results resemble previous reports (Elshatory et al., 2007; Pang et al., 2013). Calbindin D-28k is named so due to its molecular weight. The immunoblot of brain homogenates of the mouse, rat and monkey with the monoclonal antibody (Swant) (Fischer, Foster, Scott, & Sherwood, 2008; Zhang et al., 2003) revealed a single band at 28 kDa, and the immunoreactivity in the brain was absent in calbindin D-28k knockout mice. The antibody from Sigma identified a single band close to 28 kDa from MDBK cell extract. The antibody did not react with other members of the EF-hand family, such as calbindin D-9k, calretinin, myosin light chain, parvalbumin, S-100a, S-100b, S-100A2 (S100L) and S-100A6 (calcyclin). The monoclonal anti-PSD-95 antibody identified a heavy band at 95 kDa and a weak band at ~ 75 kDa. The monoclonal anti-GNB5 recognized a single band at 32.5 kDa, close to the predicted molecular weight of 28 kDa. Monoclonal anti-SV2 antibody recognizes all 3 isoforms, SV2A, B & C (Fischer et al., 2008; Bejarano-Escobar et al., 2012). Anti-PSD-95 (Ivanova, Toychiev, Yee, & Sagdullaev, 2013; Fischer et al., 2008) and anti-GNB5 have been previously used to identify synapses in retinal neurons and synapses in ON BCs (Mojumder et al., 2009; Morgans et al., 2007). The specificity of the primary antibodies has also been demonstrated in the previous studies and they provided similar staining patterns in our results. The anti-mGluR6 antibody from Santa Cruz revealed a band at the predicted molecular weight of 92–110 kDa consistent with mGluR6 (Yao et al., 2005). The anti-mGluR6 antibody from Neuromics labeled the invaginating processes of cone and rod photoreceptors (Gregg et al., 2007; Oh et al., 2007) and recognized a single band around 100 kDa from mouse retinal lysates. Our data (Fig. 8) showed that the mGluR6 immunoreactivity in the outer plexiform layer (OPL) was absent in mGluR6 knockout mice, demonstrating the labeling specificity. The technical details for the antibodies can be found in the table and manufactures' websites and data sheets. Fluorescein labeled PNA (1: 50, Vector Laboratories, Burlingame, CA) was used in the primary antibody diluents. It specifically labeled cones as previously reported (Blanks & Johnson, 1984; Wassle et al., 2009; Vandenberghe et al., 2013). Further information for antibodies was included in the Table.

Immunocytological labeling

For labeling individual mouse cones with NB, the freshly dissected whole retinas were mounted in a recording chamber containing oxygenated Ames medium (Sigma-Aldrich) and maintained at room temperature. 1% neurobiotin (NB, MW 322.85; Vector Laboratories, Burlingame, CA) in the internal solution made for physiological recording (Pang et al., 2010) was delivered into the outer limiting membrane with a micropipette of a resistance of ~ 6 MΩ by a brief positive pressure of 1 sec and 25 mmHg. 3–5 injections were made at different regions in each whole retina. Individual labeled cones were often found at edges of injection sites. Other procedures followed previously established protocols (Pang et al., 2013; Pang et al., 2010). The retinas were fixed 30 minutes after the injection.

All fixed retinas were further blocked with 10% donkey serum (Jackson ImmunoResearch, West Grove, PA) in TBS (D-PBS with 0.5% Triton X-100 (Sigma-Aldrich) and 0.1% NaN3 (SigmaAldrich)) for 2 hours at room temperature or at 4°C overnight to reduce nonspecific labeling. A vibratome (Pelco 102, 1000 Plus; Ted Pella, Inc., Redding, CA) was used to prepare retinal slices. Whole retinas were imbedded in low gel-point agarose (Sigma-Aldrich) and trimmed into a 10×10×10 mm^3 block. The block was glued onto a specimen chamber mounted on the vibratome and subsequently cut into 40-μm thick vertical sections in PBS solution. Whole retinas and free-floating sections were incubated in primary antibodies in the presence of 3% donkey serum-TBS for 3 to 5 days in 4°C. Controls were also processed without primary antibodies. Following several rinses, the slices and whole retinas were then transferred into Cy3-, Cy5-, or Alexa Fluor 488-conjugated streptavidin (1:200, Jackson ImmunoResearch), with Cy3- and/or Cy5-conjugated secondary antibodies (1:200, Jackson ImmunoResearch) and/or Alexa Fluor 488-conjugated secondary antibodies (1:200; Molecular Probes, Eugene, OR), in 3% normal donkey serum-TBS solution at 4°C overnight. A nuclear dye, TO-PRO-3 (0.5 μL/mL, Molecular Probes, Eugene, Oregon) was used with the secondary antibody to visualize nuclei in retinas. After extensive rinsing, the retinal preparations were cover-slipped. Two small pieces of filter paper (180-μm thick, MF-membrane filters; Millipore, Billerica, MA) were mounted beside whole retinas to prevent them from being over-flattened. All samples for confocal microscopy were never dehydrated.

Zeiss confocal microscopes (LSM 510 and LSM 800, Carl Zeiss, Germany) along with the imaging software were used to examine cone-RBC synapses and take images. We examined putative cone-RBC contacts in confocal optical sections crossing entire cone pedicles with a vertical resolution of 0.4–1.0 μm under regular line-scan and frame-scan modes. Potential synaptic contacts were also studied in 1–2-μm-thick blocks using confocal Airyscan protocol and software with a resolution of 30 nm per pixel. These Airyscan images were displayed by the 3D surface profile reconstructed from a series of optical sections obtained with a step of 150–180 nm (Fig. 8). For better visibility, images were presented against either black or white background. The white background was achieved simply by inverting the image of black background using Photoshop software (Adobe Systems Incorporated, San Jose, CA). Red-green images with only two active channels were further converted to magenta-green by copying the red channel to the originally blank blue channel, so that the double-labeled profiles appeared in black color (Fig. 2–4 and 6–7), yielding optimal clarity and contrast for easy observation of light-adapted human eyes.

Statistical analysis

Data were analyzed by Sigmaplot software v12 (Systat, Point Richmond, CA) and Microsoft Excel and presented as *mean ± s.e.* Two-tail Student *t*-test was used for analyzing statistical significance between data groups. And α level to reject the null hypothesis is 0.05.

Results

Identification of RBCs, rod and cone photoreceptors and photoreceptor synapses

PKCα antibody specifically labeled mouse and baboon RBCs, including their somas, dendrites and axon terminals. Mouse RBC axon terminals ramified only in the sublamina b of the inner plexiform layer, possessing 2–3 enlarged polymorphic narrow-field branches situated close to the ganglion cell layer (GCL) (Greferath et al., 1990; Kolb et al., 1993; Behrens, Kasten, & Wagner, 1998). For NB-labeled mouse preparations, only those containing distinguishable individual cones and rods were chosen for this study (Fig. 1–3). NB-filled cones showed large somas of ~ 5 × 10 (minor × major axis) μm, located in the first soma row in the outer nuclear layer (ONL). Each cone showed a single triangular shaped pedicle ~5 μm wide, which further sent out several telodendrites (Fig. 1–3). NB-filled rods had smaller somas, distributed throughout the ONL. Their axonal terminals (spherules) appeared to be spherical or oval and ~ 2 μm in diameter. Rod inner segments had nearly even thickness and were about 50% thinner than most cone inner segments (Fig. 1). These anatomical features allowed us to reliably distinguish individual cones from rods in NB-labeled mouse retinas. In baboon retinas, cone pedicles and outer segments were positive for calbindin D-28k, while rods were negative (Fig. 5–7). Both mouse and baboon cone pedicles were also labeled by PNA. Cone-RBC contacts were identified as synaptic contacts by observation of 1) RBC dendrites deeply invaginating into the center of cone pedicles (invaginating synapses) (Fig. 2–3, 6–7), 2) RBC dendritic spines plugging into the surface of cone pedicles (superficial synapses) (Fig.2, 3, 7), and/or 3) PKCα-immunoreactivity coinciding with synaptic marker (SV2, PSD-95, mGluR6 or GNB5) and cone marker (PNA or calbindin D-28k) (Fig. 4 and 6–8). Possessing one of such RBC-cone contact qualified both the RBC and cone to be counted in this study. Parallel overlapping of RBC dendrites with the surface of cone pedicles were not identified as cone-RBC contacts/synapses. Baboon retinas without a PKCα-positive band in the center of the IPL were chosen for this study to avoid DB4 cone bipolar cells.

RBCs received both superficial and invaginating synapses from cone pedicles

PNA brightly labeled cone inner segments and cone pedicles. In mouse retinal slices, PNA-positive profiles in the OPL appeared as short “bars” nearly parallel to the OPL (Fig. 4). Using R/G-opsin antibody and NB to visualize the complete morphology of individual mouse cones, this study observed that each bar-shaped PNA immunoreactivity belonged to the basal membrane of R/G cone pedicles. In retinal slices and flat-mounts, mouse (Fig. 1–3) and baboon (Fig. 5–6) cone pedicles were observed to send out several telodendrites (Kraft & Burkhardt, 1986; Wassle et al., 2009) to the adjacent regions. In double- or tripled labeled retinas, PNA signals colocalized with those of synaptic marker SV2 (Fig. 4), and these cone synapses were situated the closest to the bipolar soma layer and in the most proximal region of the OPL among all synapses labeled there. RBC dendrites were found to make both invaginating and superficial synaptic contacts with cone pedicles in mouse (Fig. 2–4) and baboon retinas (Fig. 6–8). Some PKCα-immunoreactivity was found to deeply penetrate to the center or protrude into the surface of cone pedicles (Fig. 2–3 and 6–7) and colocalize SV2 (Fig. 4C) and PSD-95 signal (Fig. 6–7) in cone pedicles. In the mouse retina, RBC dendritic terminals mostly invaginated to the center of SV2-labeled rod spherules, appearing

like pomegranate arils (Fig. 4C). These rod-RBC synapses were located farther from RBC somas compared with cone-RBC synapses.

Superficial RBC-cone contacts were predominant, particularly in the baboon retina. But unlike invaginating contacts which were often restricted to the basal membrane (Fig. 2 and 7), superficial contacts were found in the basal and side membranes of cone pedicles (Fig. 2, 3, 6–8), as well as in telodendrites (Fig. 3 and 6), for both mouse and baboon retinas. Similar to mouse rod spherules, one cone pedicle could receive 0–1 invaginating dendritic terminal from a RBC. However, 1–3 superficial contacts were found for one RBC in both mouse and baboon retinas. On the other hand, one cone could contact 1–3 RBCs. Mouse RBCs that contacted cones showed similar lengths to other RBCs. The total length of the soma and axon was 101.1 ± 2.5 μm (n= 14 cells) compared with 104.9 ± 1.5 μm (n=14 cells) in other RBCs (two-tail p=0.091).

To count RBCs and cones that contacted each other, we took consecutive optical images with a resolution of 0.4–1.0 μm from triple-labeled retinas. In randomly selected images, we counted intensively PKCα-positive somas located in the first and second soma row in the inner nuclear layer as RBCs. PKCα-positive dendrites that contacted cones were traced back to the soma to confirm the RBC identity. Cone pedicles labeled by PSD-95 or calbindin D-28k were counted as the total number of cones. In PNA-labeled retinas, cones were counted by the clusters of bright PNA signals in the OPL. The percentage of RBCs that contacted cones were calculated by the number of these RBCs being divided by the total number of RBCs, and that of cones were calculated by the number of cones that contacted RBCs being divided by the total number of cones in the same images. High-resolution confocal consecutive images were taken over individual cone pedicles and RBCs to determine how many RBC-cone contacts were present on each RBC and each cone.

Up to half of RBCs and cones contact each other in the mouse retina

The data showed that 38.9% ± 0.04% (46/120) of RBCs in the central retina contacted cones, while fewer RBCs did in the peripheral retina (20.7% ± 0.03%, 25/123) (p=0.009, n=14 samples), yielding an average value of 29.8%. The percentage of cones that contacted RBCs was not significantly different between the central and peripheral retina (48.5% ± 0.05% (42/87) and 34.3% ± 0.05%(25/74) respectively) (p=0.07, n=14 samples). Cone-RBC contacts were observed from all retinas examined. Data from retinas differentially labeled were not separately analyzed, except mouse retinas labeled for GNB5 (see below).

Cone-RBC contacts involved nearly 10% of RBCs and 20 % of cones in the baboon retina

PKCα-labeled RBCs in baboon retinas also showed similar contacts with cones, but less frequently. PKCα-positive cells were identified as RBCs by their intensive PKCα-immunoreactivity and the morphology of axonal terminals. Diffuse cone bipolar cells (DB4) may be weakly labeled for PKCα (Grunert, Martin, & Wassle, 1994; Mills & Massey, 1999) but not on all occasions (Grunert & Martin, 1991). Their axonal terminals ramify at 40%–60% of the IPL depth, forming a band separated from those of RBCs in the IPL. We distinguished RBCs from DB4 cells by the morphology of their axon terminals and contacts with rods in the dendrites (Fig. 7). In our experimental conditions, only a smaller number of

retinal preparations showed the extra PKCα-positive band, and this study only used retinal slices without the extra band (Fig. 6–7) to avoid DB4 cells.

The entire cone including the pedicle in the baboon retina was positively labeled for calbindin D-28k. The pedicles showed a fat sock-like shape (Fig. 6–7) in retinal slices, similar to cone pedicles observed in the human retina by others (Zhang et al., 2003). They were nearly 5 μm wide and 10 μm tall. PKCα-positive RBC dendrites were found to contact the lower portion of cone pedicles. PNA signals in the OPL were weaker in the baboon retina compared to the mouse retina. They appeared as puncta and primarily arranged as small clusters and concentrated in the basal membrane of cone pedicles (Fig. 5–8). Each cluster belonged to one cone pedicle (Fig. 5–6). Bright PNA puncta were also found in endings of cone telodendrites (Fig. 5). Each PNA-labeled cone pedicle sent out several radiating telodendrites These telodendrites often attached to the pedicle by thinner processes and expanded at the end, and they were better visualized in overexposed images in both retinal slices and flat-mounts (Fig. 5). Some PNA signals were found to coincide with RBC dendrites. In PKCα and PSD-95 double-labeled retinas (Fig. 6G and 7), PKCα-positive bipolar cell dendrites contacted large cone-shaped PSD-95-positive cone pedicles and small oval-shaped rod spherules in a similar way; the axon terminals of the bipolar cells ramified at ~70 to 100% of the IPL depth, and individual cells showed contacts with both cones and rods (Fig. 7). These data demonstrate that RBCs may contact cones. 22.49% ± 0.02% of cones (n= 225) contacted RBCs. RBCs that contacted cones accounted for 12.17% ± 0.01% of the cells (n= 416), and they slightly favorited the para-central retina compared to the peripheral retina ($P>0.05$, n=2 samples). Cone-RBC contacts were observed from all retinal preparations differentially labeled.

The expression of mGluR6 and G protein subunit beta 5 (GNB5) in contacts between cones and RBCs

GNB5 has been reported to colocalize with mGluR6 in mammalian retinas (Mojumder et al., 2009; Morgans et al., 2007). To further confirm synapses formed by cones and RBCs, we triple-labeled retinas using mGluR6 or GNB5 antibodies with PKCα and PNA or calbindin-28k antibodies (Fig. 8). The results showed that GNB5 and mGluR6 were present in the contacts between cone pedicles and PKCα-labeled RBC dendrites (Fig. 8). In the mouse retina, 29.5% PKCα–positive RBCs (18/61 cells) contacted cones, and GNB5 was present in these contacts. This result was consistent with the data described in previous sections (29.8%). In the baboon retinas (n=2), both mGluR6 and GNB5 were found in RBC-cone contacts.

In mGluR6 knockout mice, mGluR6 immunoreactivity in the outer plexiform layer was absent. Some large punctate labeling in the inner and outer nuclear layers remained. It indicates that the labeling of mGluR6 in the OPL was specific (Fig. 8).

Discussion

This study observed cone-RBC synapses in the mouse and primate retina, providing anatomical evidence for previously revealed cone chemical synaptic inputs in mouse RBCs (Pang et al., 2010). Our data also revealed that mouse RBCs received cone contacts more

frequently than primate RBCs, indicating these RBCs are functionally more important for nocturnal animals. Additionally, mouse RBCs were found to contact cones more frequently in the central retina than in the peripheral retina, consistent with the cone distribution peak in the central retina (Ortin-Martinez et al., 2014; Jeon, Strettoi, & Masland, 1998).

The results showed that cone-RBC synaptic contacts involved about 10% of RBCs and 20% of cones in baboon retinas and nearly 30% of RBCs and 40% of cones in the mouse retina. One RBC could form 0–1 invaginating and 1–3 superficial contacts with cones, while one cone could contact 1–3 RBCs. These data are well in line with the report from the mouse retina (Behrens et al., 2016), though the RBC population contacting cones of the mouse retina in this report is smaller than in that recent study (Behrens et al., 2016). The difference is possibly related to the difficulty in identifying RBCs and synapses. Immunocytochemistry and confocal microscopy generally have a lower resolution than electron microscopy (Behrens et al., 2016; Helmstaedter et al., 2013) for identifying synapses and can possibly cause an underestimation of the synapses. On the other hand, the former allows better identification of RBCs by their PKCα-immunoreactivity. Additionally, in this study all retinal preparations were never dehydrated, preventing examiners from mistaking physical contacts induced by artificial tissue deformation as synaptic contacts. Nevertheless, these data demonstrate that mammalian RBCs can integrate rod and cone signals.

In recent decades, confocal microscopy and immuno-markers have been widely used for studying rod and cone synapses. RBCs are often identified by a classic marker PKCα antibody, and cone pedicles are often identifiable by other immuno-markers, such as PNA (Wassle et al., 2009; Kraft & Burkhardt, 1986), GluR5 (Wassle et al., 2009), and glycogen phosphorylase (Wassle et al., 2009; Pfeiffer-Guglielmi, Fleckenstein, Jung, & Hamprecht, 2003). Similar approaches were used in this study, in conjunction with synaptic markers SV2, PSD-95, mGluR6 and GNB5. In addition, we were able to visualize the entire cone morphology and the boundary of cone pedicles by neurobiotin-labeling, as well as the staining for red/green (R/G) opsin. Anti-R/G-opsin antibody was used to label all mouse cones, because mouse cones all express M-opsin (λ_{max}=508 nm) (Rohlich, van, & Szel, 1994; Applebury et al., 2000).

In mammals, up to 13 morphological subtypes of cone bipolar cells have been identified, however, all RBCs belong to a single anatomical subtype. Previous data supporting this concept were obtained from light and electron microscopic studies in the cat, rabbit and primate retinas. RBCs across species show a similar morphology, as has been well described from Golgi-impregnated retinas (Cajal, 1893; Polyak, 1941; Boycott & Kolb, 1973; Boycott & Dowling, 1969). The synaptic connections of RBCs in the inner plexiform layer (IPL) of the cat (Kolb & Famiglietti, 1974; McGuire, Stevens, & Sterling, 1984; Freed, Smith, & Sterling, 1987; Kolb, 1979), rabbit (Raviola & Raviola, 1967; Raviola & Dacheux, 1987; Strettoi et al., 1990; Grunert & Martin, 1991) and primate (Boycott & Dowling, 1969; Boycott & Kolb, 1973; Grunert & Martin, 1991) appear to have the same general organization. Although in electron microscopic studies PKCα-positive RBC dendrites have been observed to invaginate into cone pedicles in primate (Grunert & Martin, 1991) and rabbit retinas (Dacheux & Raviola, 1986), they were not statistically studied owing to their low frequency. Here, our data show that cone-RBC contacts are present in 30% of mouse

RBCs and in nearly 10% of primate RBCs. Such RBCs could make 0–1 invaginating contact with cones. The single RBC invaginating contact in cones was comparable with that in rods revealed in both this study (Fig.3, 4, 6 and 7) and others' reports (Dacheux & Raviola, 1986; Grunert & Martin, 1991; Kolb, 1970). In addition, our results show that RBCs primarily make superficial contacts with cones. Based on cone signals recorded from DBC_{R2} in the mouse retina (Pang et al., 2010) and cone-RBC contacts revealed in this and other studies (Grunert & Martin, 1991; Dacheux & Raviola, 1986), we speculate that cone-RBC synapses have physiological impact in mammalian retinas.

In the primate retina, we observed that some PKCα-positive bipolar cells received both rod and cone synapses, demonstrating the presence of RBC-cone contacts. Although DB4 cells are positive for PKCα, they are known not to receive rod inputs (Hopkins & Boycott, 1995; Grunert et al., 1994; Tsukamoto & Omi, 2016). Rod bipolar cells are intensively PKCα-positive (Greferath et al., 1990; Kolb et al., 1993; Wassle et al., 2009), while DB4 cells are weakly PKCα–positive (Grunert et al., 1994), especially the soma and dendrites (Sulaiman, Fina, Feddersen, & Vardi, 2010). Meanwhile, many (Lassova, Fina, Sulaiman, & Vardi, 2010) DB4 cells, or all of them in some experimental conditions (Grunert & Martin, 1991), are not stained for PKCα. This study chose retinas without the PKCα-band in the center of the IPL. And we encountered more superficial contacts between PKCα-positive dendrites and cones, while a great majority of DB4 cells makes invaginating synapses with cones (Hopkins & Boycott, 1995). Therefore, we believe that RBC-cone contacts that we identified are not DB4-cone contacts.

Primate retinas (Curcio, Sloan, Kalina, & Hendrickson, 1990; Schneeweis & Schnapf, 1995) possess a higher cone : rod ratio, while nocturnal animals like mice have a lower cone : rod ratio (Jeon et al., 1998). And rabbit retinas show a higher cone bipolar cell : RBC ratio (3–4: 1), but the ratio is lower in the mouse retina (2.6 : 1) (Strettoi & Volpini, 2002; Wassle et al., 2009). Whether the relatively large RBC pool in the mouse retina has more complex functions is still unclear. OFF bipolar cells in the mammalian retina had been previously understood as typical cone bipolar cells because only RBCs were known to be driven by rods. However, in the recent two decades, both anatomical and physiological evidence has emerged, confirming rod inputs to OFF bipolar cells. In mouse retinas, nearly 4 anatomical subtypes (type 1, 2, 3a, 3b and 4) and 3 physiological subtypes ($HBC_{R/MC}$, HBC_{MC}, $HBC_{M/SC}$) of OFF BCs have been identified, based on their axon terminal morphology, immunoreactivity and location in the IPL (Ghosh, Bujan, Haverkamp, Feigenspan, & Wassle, 2004; Pignatelli & Strettoi, 2004; Wassle et al., 2009), and waveform and sensitivity of their light responses (Pang et al., 2012; Arman & Sampath, 2012). Both type 3a and 3b OFF BCs form flat contacts at cone pedicles and rod spherules (Mataruga, Kremmer, & Muller, 2007). And some calsenilin-positive dendrites from type 4 OFF BCs contact rods, as well (Haverkamp et al., 2008). Dendrites of DB3b OFF BCs made contact with both rods and cones at the photoreceptor basal surface in the macaque retina (Tsukamoto & Omi, 2014). The current finding, along with previous anatomical and physiological data together, consistently indicate that mammalian retinal second-order neurons can receive rod-cone mixed inputs. Therefore, mammalian retinal second order neurons may pass both segregated rod and cone signals and integrated rod and cone signals to retinal third order neurons.

In mesopic conditions, rods become saturated and cones are barely activated. Since rod/cone-driven RBCs integrate rod and cone inputs, they appear to be able to mediate mammalian mesopic vision, enabling smooth mode-shifting between night vision and photopic vision. In the mammalian retina, ON ganglion cells receive rod signals mainly from the primary rod pathway via cone bipolar cell chemical synapses, because mammalian RBCs do not directly contact ON ganglion cells. Only recently were some mammalian cone ON bipolar cells found to receive mixed rod-cone inputs (Pang et al., 2010). AII amacrine cells have been identified as a critical mediator for the primary rod pathway (Dowling, 2012; Masland, 2012; Bloomfield & Volgyi, 2009). These cells form electric contacts with cone bipolar cells and receive chemical synapses from RBCs at the same time, integrating cone and rod signals before they reach ON ganglion cells. In this paper our data suggest that, like AII amacrine cells, some RBCs could integrate rod and cone signals, sharing the duty of shaping rod and cone inputs in ON ganglion cells.

Acknowledgments

This work is supported by NIH (EY 019908, EY004446), NIH Vision Core (02520), the Retina Research Foundation (Houston), and Research to Prevent Blindness, Inc.

Role of authors

All authors had full access to all the data in the study and take responsibility for the integrity of the data and the accuracy of the data analysis. Study concept and design: JJP. Acquisition of data: JJP and YZ. Analysis and interpretation of data: JJP and SMW. Drafting of the manuscript: JJP. Critical revision of the manuscript for important intellectual content: JJP, RAJ and SMW. Statistical analysis: JJP and YZ. Obtained funding: SMW. Administrative, technical, and material support: YZ, RAJ and SMW. Study supervision: SMW and JJP.

Literature Cited

Aartsen WM, Kantardzhieva A, Klooster J, van Rossum AG, van de Pavert SA, Versteeg I, et al. Mpp4 recruits Psd95 and Veli3 towards the photoreceptor synapse. Hum. Mol. Genet. 2006; 15:1291–1302. [PubMed: 16520334]

Applebury ML, Antoch MP, Baxter LC, Chun LL, Falk JD, Farhangfar F, et al. The murine cone photoreceptor: a single cone type expresses both S and M opsins with retinal spatial patterning. Neuron. 2000; 27:513–523. [PubMed: 11055434]

Arman AC, Sampath AP. Dark-adapted response threshold of OFF ganglion cells is not set by OFF bipolar cells in the mouse retina. J. Neurophysiol. 2012; 107:2649–2659. [PubMed: 22338022]

Bajjalieh SM, Peterson K, Shinghal R, Scheller RH. SV2, a brain synaptic vesicle protein homologous to bacterial transporters. Science. 1992; 257:1271–1273. [PubMed: 1519064]

Behrens C, Schubert T, Haverkamp S, Euler T, Berens P. Connectivity map of bipolar cells and photoreceptors in the mouse retina. Elife. 2016; 5

Behrens UD, Kasten P, Wagner HJ. Adaptation-dependent plasticity of rod bipolar cell axon terminal morphology in the rat retina. Cell Tissue Res. 1998; 294:243–251. [PubMed: 9799440]

Bejarano-Escobar R, Blasco M, Duran AC, Rodriguez C, Martin-Partido G, Francisco-Morcillo J. Retinal histogenesis and cell differentiation in an elasmobranch species, the small-spotted catshark Scyliorhinus canicula. J. Anat. 2012; 220:318–335. [PubMed: 22332849]

Blanks JC, Johnson LV. Specific binding of peanut lectin to a class of retinal photoreceptor cells. A species comparison. Invest Ophthalmol. Vis. Sci. 1984; 25:546–557. [PubMed: 6715128]

Bloomfield SA, Volgyi B. The diverse functional roles and regulation of neuronal gap junctions in the retina. Nat. Rev. Neurosci. 2009; 10:495–506. [PubMed: 19491906]

Boycott BB, Dowling JE. Organization of the primate retina: light microscopy. Philos. Trans. R. Soc. Lond. (Biol.). 1969; 255:109–184.

Boycott BB, Kolb H. The horizontal cells of the rhesus monkey retina. J. Comp Neurol. 1973; 148:115–139. [PubMed: 4121525]

Cajal S. La rétine des vertébrés. Cellule. 1893; 9:121–255. Ref Type: Abstract.

Curcio CA, Sloan KR, Kalina RE, Hendrickson AE. Human photoreceptor topography. J. Comp Neurol. 1990; 292:497–523. [PubMed: 2324310]

Dacheux RF, Raviola E. The rod pathway in the rabbit retina: a depolarizing bipolar and amacrine cell. J. Neurosci. 1986; 6:331–345. [PubMed: 3950701]

Dowling, JE. The Retina an approachable part of the brain. Cambridge: Harvard University Press/ Belknap Press; 2012.

El-Husseini AE, Schnell E, Chetkovich DM, Nicoll RA, Bredt DS. PSD-95 involvement in maturation of excitatory synapses. Science. 2000; 290:1364–1368. [PubMed: 11082065]

Elshatory Y, Everhart D, Deng M, Xie X, Barlow RB, Gan L. Islet-1 controls the differentiation of retinal bipolar and cholinergic amacrine cells. J. Neurosci. 2007; 27:12707–12720. [PubMed: 18003851]

Euler T, Haverkamp S, Schubert T, Baden T. Retinal bipolar cells: elementary building blocks of vision. Nat. Rev. Neurosci. 2014; 15:507–519. [PubMed: 25158357]

Feany MB, Lee S, Edwards RH, Buckley KM. The synaptic vesicle protein SV2 is a novel type of transmembrane transporter. Cell. 1992; 70:861–867. [PubMed: 1355409]

Fischer AJ, Foster S, Scott MA, Sherwood P. Transient expression of LIM-domain transcription factors is coincident with delayed maturation of photoreceptors in the chicken retina. J. Comp Neurol. 2008; 506:584–603. [PubMed: 18072193]

Freed MA, Smith RG, Sterling P. Rod bipolar array in the cat retina: pattern of input from rods and GABA-accumulating amacrine cells. J. Comp Neurol. 1987; 266:445–455. [PubMed: 3693619]

Fyk-Kolodziej B, Qin P, Pourcho RG. Identification of a cone bipolar cell in cat retina which has input from both rod and cone photoreceptors. J. Comp Neurol. 2003; 464:104–113. [PubMed: 12866131]

Ghosh KK, Bujan S, Haverkamp S, Feigenspan A, Wassle H. Types of bipolar cells in the mouse retina. J. Comp Neurol. 2004; 469:70–82. [PubMed: 14689473]

Greferath U, Grunert U, Wassle H. Rod bipolar cells in the mammalian retina show protein kinase C-like immunoreactivity. J. Comp Neurol. 1990; 301:433–442. [PubMed: 2262600]

Gregg RG, Kamermans M, Klooster J, Lukasiewicz PD, Peachey NS, Vessey KA, et al. Nyctalopin expression in retinal bipolar cells restores visual function in a mouse model of complete X-linked congenital stationary night blindness. J. Neurophysiol. 2007; 98:3023–3033. [PubMed: 17881478]

Grunert U, Martin PR. Rod bipolar cells in the macaque monkey retina: immunoreactivity and connectivity. J. Neurosci. 1991; 11:2742–2758. [PubMed: 1715391]

Grunert U, Martin PR, Wassle H. Immunocytochemical analysis of bipolar cells in the macaque monkey retina. J. Comp Neurol. 1994; 348:607–627. [PubMed: 7530731]

Hack I, Peichl L, Brandstatter JH. An alternative pathway for rod signals in the rodent retina: rod photoreceptors, cone bipolar cells, and the localization of glutamate receptors. Proc. Natl. Acad. Sci. U. S. A. 1999; 96:14130–14135. [PubMed: 10570210]

Haverkamp S, Specht D, Majumdar S, Zaidi NF, Brandstatter JH, Wasco W, et al. Type 4 OFF cone bipolar cells of the mouse retina express calsenilin and contact cones as well as rods. J. Comp Neurol. 2008; 507:1087–1101. [PubMed: 18095322]

Helmstaedter M, Briggman KL, Turaga SC, Jain V, Seung HS, Denk W. Connectomic reconstruction of the inner plexiform layer in the mouse retina. Nature. 2013; 500:168–174. [PubMed: 23925239]

Hopkins JM, Boycott BB. Synapses between cones and diffuse bipolar cells of a primate retina. J. Neurocytol. 1995; 24:680–694. [PubMed: 7500123]

Ivanova E, Toychiev AH, Yee CW, Sagdullaev BT. Optimized protocol for retinal wholemount preparation for imaging and immunohistochemistry. J. Vis. Exp. 2013:e51018. [PubMed: 24379013]

Jacoby R, Stafford D, Kouyama N, Marshak D. Synaptic inputs to ON parasol ganglion cells in the primate retina. J. Neurosci. 1996; 16:8041–8056. [PubMed: 8987830]

Jeon CJ, Strettoi E, Masland RH. The major cell populations of the mouse retina. J. Neurosci. 1998; 18:8936–8946. [PubMed: 9786999]

Joo HR, Peterson BB, Haun TJ, Dacey DM. Characterization of a novel large-field cone bipolar cell type in the primate retina: evidence for selective cone connections. Vis. Neurosci. 2011; 28:29–37. [PubMed: 21156090]

Kolb H. Organization of the outer plexiform layer of the primate retina: electron microscopy of Golgi-impregnated cells. Philos. Trans. R. Soc. Lond B Biol. Sci. 1970; 258:261–283. [PubMed: 22408829]

Kolb H. The inner plexiform layer in the retina of the cat: electron microscopic observations. J. Neurocytol. 1979; 8:295–329. [PubMed: 490185]

Kolb H, Famiglietti EV. Rod and cone pathways in the inner plexiform layer of cat retina. Science. 1974; 186:47–49. [PubMed: 4417736]

Kolb H, Zhang L, Dekorver L. Differential staining of neurons in the human retina with antibodies to protein kinase C isozymes. Vis. Neurosci. 1993; 10:341–351. [PubMed: 8485096]

Koulen P, Fletcher EL, Craven SE, Bredt DS, Wassle H. Immunocytochemical localization of the postsynaptic density protein PSD-95 in the mammalian retina. J. Neurosci. 1998; 18:10136–10149. [PubMed: 9822767]

Kraft TW, Burkhardt DA. Telodendrites of cone photoreceptors: structure and probable function. J. Comp Neurol. 1986; 249:13–27. [PubMed: 2426311]

Lassova L, Fina M, Sulaiman P, Vardi N. Immunocytochemical evidence that monkey rod bipolar cells use GABA. Eur. J. Neurosci. 2010; 31:685–696. [PubMed: 20384812]

Li W, Chen S, DeVries SH. A fast rod photoreceptor signaling pathway in the mammalian retina. Nat. Neurosci. 2010; 13:414–416. [PubMed: 20190742]

Li W, Keung JW, Massey SC. Direct synaptic connections between rods and OFF cone bipolar cells in the rabbit retina. J. Comp Neurol. 2004; 474:1–12. [PubMed: 15156575]

Masland RH. The neuronal organization of the retina. Neuron. 2012; 76:266–280. [PubMed: 23083731]

Masu M, Iwakabe H, Tagawa Y, Miyoshi T, Yamashita M, Fukuda Y, et al. Specific deficit of the ON response in visual transmission by targeted disruption of the mGluR6 gene. Cell. 1995; 80:757–765. [PubMed: 7889569]

Mataruga A, Kremmer E, Muller F. Type 3a and type 3b OFF cone bipolar cells provide for the alternative rod pathway in the mouse retina. J. Comp Neurol., %20;. 2007; 502:1123–1137. [PubMed: 17447251]

McGuire BA, Stevens JK, Sterling P. Microcircuitry of bipolar cells in cat retina. J. Neurosci. 1984; 4:2920–2938. [PubMed: 6502212]

Mills SL, Massey SC. AII amacrine cells limit scotopic acuity in central macaque retina: A confocal analysis of calretinin labeling. J. Comp Neurol. 1999; 411:19–34. [PubMed: 10404105]

Mojumder DK, Qian Y, Wensel TG. Two R7 regulator of G-protein signaling proteins shape retinal bipolar cell signaling. J. Neurosci. 2009; 29:7753–7765. [PubMed: 19535587]

Morgans CW, Wensel TG, Brown RL, Perez-Leon JA, Bearnot B, Duvoisin RM. Gbeta5-RGS complexes co-localize with mGluR6 in retinal ON-bipolar cells. Eur. J. Neurosci. 2007; 26:2899–2905. [PubMed: 18001285]

O'Brien J, Nguyen HB, Mills SL. Cone photoreceptors in bass retina use two connexins to mediate electrical coupling. J. Neurosci. 2004; 24:5632–5642. [PubMed: 15201336]

Oh EC, Khan N, Novelli E, Khanna H, Strettoi E, Swaroop A. Transformation of cone precursors to functional rod photoreceptors by bZIP transcription factor NRL. Proc. Natl. Acad. Sci. U. S. A. 2007; 104:1679–1684. [PubMed: 17242361]

Ortin-Martinez A, Nadal-Nicolas FM, Jimenez-Lopez M, Alburquerque-Bejar JJ, Nieto-Lopez L, Garcia-Ayuso D, et al. Number and distribution of mouse retinal cone photoreceptors: differences between an albino (Swiss) and a pigmented (C57/BL6) strain. PLoS. One. 2014; 9:e102392. [PubMed: 25029531]

Pang JJ, Gao F, Lem J, Bramblett DE, Paul DL, Wu SM. Direct rod input to cone BCs and direct cone input to rod BCs challenge the traditional view of mammalian BC circuitry. Proc. Natl. Acad. Sci. U. S. A. 2010; 107:395–400. [PubMed: 20018684]

Pang JJ, Gao F, Paul DL, Wu SM. Rod, M-cone and M/S-cone inputs to hyperpolarizing bipolar cells in the mouse retina. J. Physiol. 2012; 590:845–854. [PubMed: 22219344]

Pang JJ, Gao F, Wu SM. Light-evoked current responses in rod bipolar cells, cone depolarizing bipolar cells and AII amacrine cells in dark-adapted mouse retina. J. Physiol. 2004; 558:897–912. [PubMed: 15181169]

Pang JJ, Gao F, Wu SM. Light responses and morphology of bNOS-immunoreactive neurons in the mouse retina. J. Comp Neurol. 2010; 518:2456–2474. [PubMed: 20503422]

Pang JJ, Paul DL, Wu SM. Survey on amacrine cells coupling to retrograde-identified ganglion cells in the mouse retina. Invest Ophthalmol. Vis. Sci. 2013; 54:5151–5162. [PubMed: 23821205]

Pfeiffer-Guglielmi B, Fleckenstein B, Jung G, Hamprecht B. Immunocytochemical localization of glycogen phosphorylase isozymes in rat nervous tissues by using isozyme-specific antibodies. J. Neurochem. 2003; 85:73–81. [PubMed: 12641728]

Pignatelli V, Strettoi E. Bipolar cells of the mouse retina: a gene gun, morphological study. J. Comp Neurol. 2004; 476:254–266. [PubMed: 15269969]

Polyak, SL. The retina. First. Illinois: The University of Chicago Press; 1941.

Puthussery T, Percival KA, Venkataramani S, Gayet-Primo J, Grunert U, Taylor WR. Kainate receptors mediate synaptic input to transient and sustained OFF visual pathways in primate retina. J. Neurosci. 2014; 34:7611–7621. [PubMed: 24872565]

Puthussery T, Venkataramani S, Gayet-Primo J, Smith RG, Taylor WR. NaV1.1 channels in axon initial segments of bipolar cells augment input to magnocellular visual pathways in the primate retina. J. Neurosci. 2013; 33:16045–16059. [PubMed: 24107939]

Raviola E, Dacheux RF. Excitatory dyad synapse in rabbit retina. Proc. Natl. Acad. Sci. U. S. A. 1987; 84:7324–7328. [PubMed: 3478695]

Raviola G, Raviola E. Light and electron microscopic observations on the inner plexiform layer of the rabbit retina. Am. J. Anat. 1967; 120:403–425. [PubMed: 6037326]

Rohlich P, van VT, Szel A. Two different visual pigments in one retinal cone cell. Neuron. 1994; 13:1159–1166. [PubMed: 7946352]

Schneeweis DM, Schnapf JL. Photovoltage of rods and cones in the macaque retina. Science. 1995; 268:1053–1056. [PubMed: 7754386]

Soucy E, Wang Y, Nirenberg S, Nathans J, Meister M. A novel signaling pathway from rod photoreceptors to ganglion cells in mammalian retina. Neuron. 1998; 21:481–493. [PubMed: 9768836]

Strettoi E, Dacheux RF, Raviola E. Synaptic connections of rod bipolar cells in the inner plexiform layer of the rabbit retina. J. Comp Neurol. 1990; 295:449–466. [PubMed: 2351763]

Strettoi E, Volpini M. Retinal organization in the bcl-2-overexpressing transgenic mouse. J. Comp Neurol. 2002; 446:1–10. [PubMed: 11920715]

Sulaiman P, Fina M, Feddersen R, Vardi N. Ret-PCP2 colocalizes with protein kinase C in a subset of primate ON cone bipolar cells. J. Comp Neurol. 2010; 518:1098–1112. [PubMed: 20127818]

Tsukamoto Y, Morigiwa K, Ueda M, Sterling P. Microcircuits for night vision in mouse retina. J. Neurosci. 2001; 21:8616–8623. [PubMed: 11606649]

Tsukamoto Y, Omi N. Some OFF bipolar cell types make contact with both rods and cones in macaque and mouse retinas. Front Neuroanat. 2014; 8105:105.doi: 10.3389/fnana.2014.00105.eCollection; %2014 [PubMed: 25309346]

Tsukamoto Y, Omi N. ON Bipolar Cells in Macaque Retina: Type-Specific Synaptic Connectivity with Special Reference to OFF Counterparts. Front Neuroanat. 2016; 10:104. [PubMed: 27833534]

Vandenberghe LH, Bell P, Maguire AM, Xiao R, Hopkins TB, Grant R, et al. AAV9 targets cone photoreceptors in the nonhuman primate retina. PLoS. One. 2013; 8:e53463. [PubMed: 23382846]

Wang MM, Janz R, Belizaire R, Frishman LJ, Sherry DM. Differential distribution and developmental expression of synaptic vesicle protein 2 isoforms in the mouse retina. J. Comp Neurol. 2003; 460:106–122. [PubMed: 12687700]

Wassle H, Puller C, Muller F, Haverkamp S. Cone contacts, mosaics, and territories of bipolar cells in the mouse retina. J Neurosci. 2009; 29:106–117. [PubMed: 19129389]

Wu-Zhang AX, Newton AC. Protein kinase C pharmacology: refining the toolbox. Biochem. J. 2013; 452:195–209. [PubMed: 23662807]

Xiong WH, Pang JJ, Pennesi ME, Duvoisin RM, Wu SM, Morgans CW. The Effect of PKCalpha on the Light Response of Rod Bipolar Cells in the Mouse Retina. Invest Ophthalmol. Vis. Sci. 2015; 56:4961–4974. [PubMed: 26230760]

Yao HH, Ding JH, Zhou F, Wang F, Hu LF, Sun T, et al. Enhancement of glutamate uptake mediates the neuroprotection exerted by activating group II or III metabotropic glutamate receptors on astrocytes. J. Neurochem. 2005; 92:948–961. [PubMed: 15686497]

Zhang H, Cuenca N, Ivanova T, Church-Kopish J, Frederick JM, Macleish PR, et al. Identification and light-dependent translocation of a cone-specific antigen, cone arrestin, recognized by monoclonal antibody 7G6. Invest Ophthalmol. Vis. Sci. 2003; 44:2858–2867. [PubMed: 12824223]

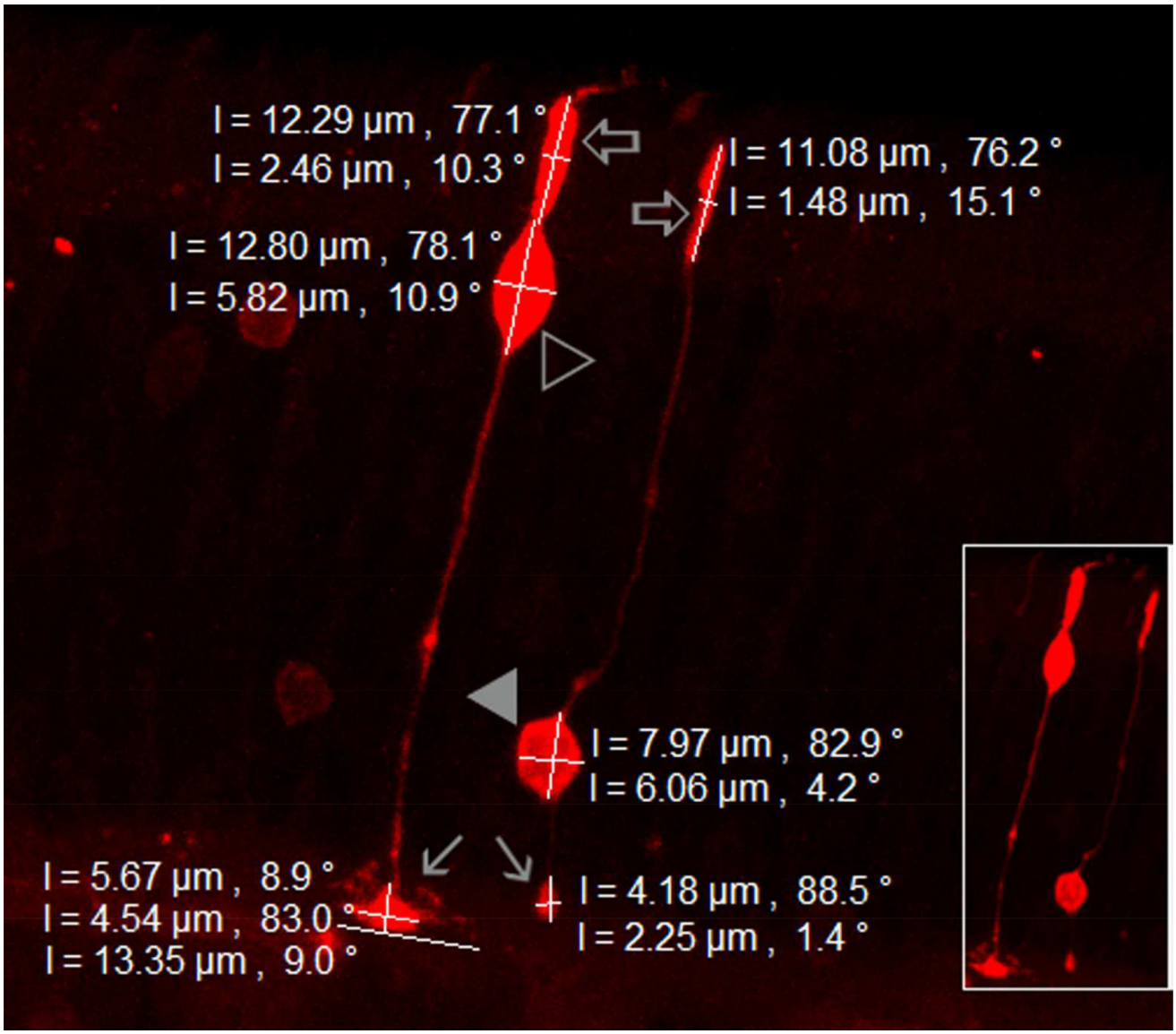

Fig.1.

Distinctive confocal morphology of individual cones and rods in the mouse retina. The stacked confocal image shows a cone and a rod filled with NB, which fully reveals the location, shape and size of the inner segments (open arrows), somas (cone-open triangle, rod-closed triangle), and axonal terminals (arrows). Zeiss imaging software was used to measure the cells. Each measure is given by a white bar with a length and an angle associated to the bar (0°-horizontal, 90°-vertical). The entire cone pedicle shows a triangular shape, which is nearly 2–7 times wider than the oval-shaped rod spherule. Cone inner segment is nearly two times thicker than the rod inner segment. The cone soma is larger than the rod soma and located near its inner segment.

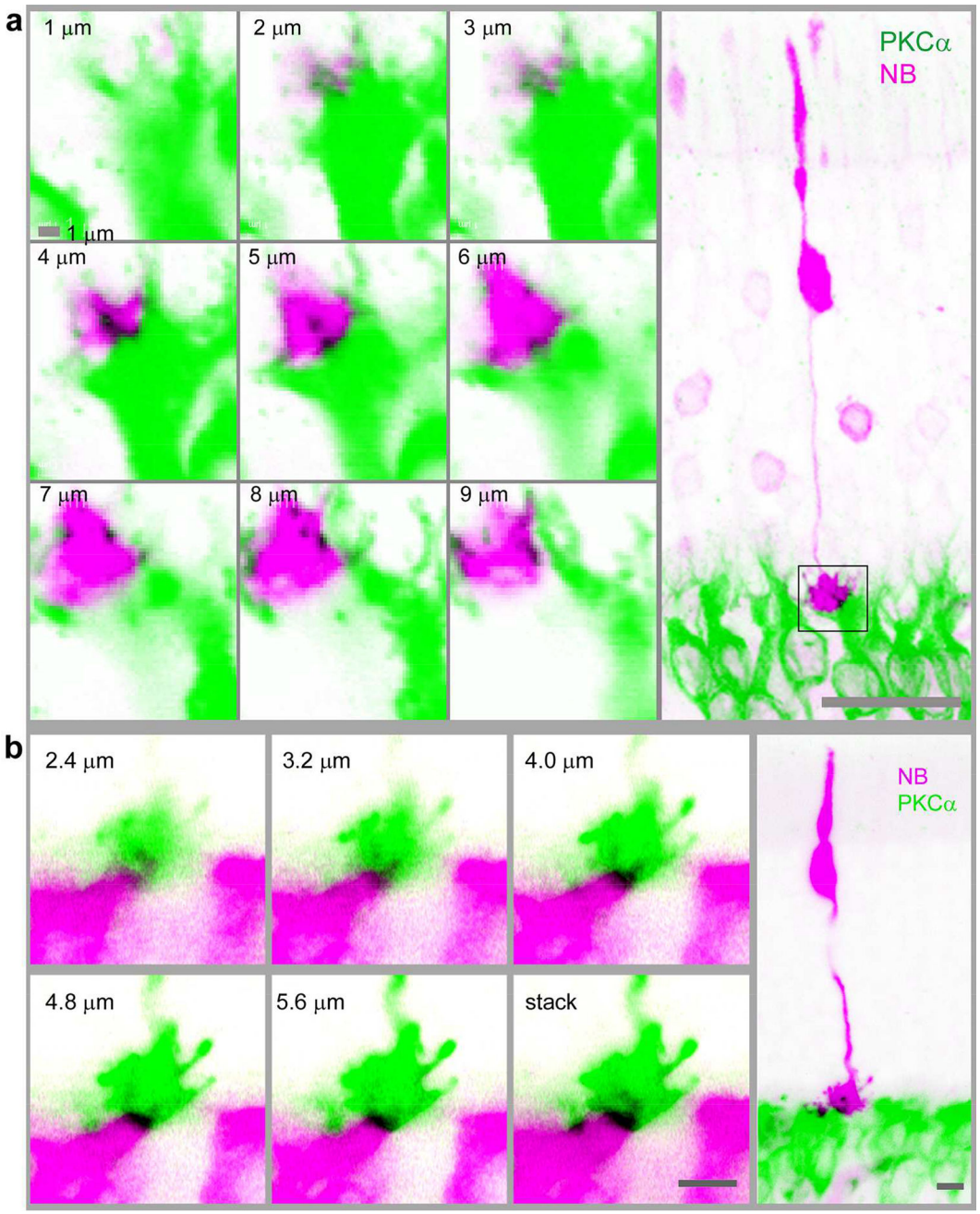

Fig. 2.

Cone-RBC synapses in the mouse retina. Cones were filled with NB (pink) in living retinas and further stained for PKCα (green). Cones possess a triangular shaped pedicle and a large soma close to its thicker inner segment (right panels). Confocal optical sections crossing cone pedicles (square region in right images) are depicted in left panels, which reveal a RBC dendrite invaginating into the center of cone pedicles (in black, in 4–5 μm (a) and 2.4–4.8 μm (b) focal planes). Consecutive confocal optical sections reveal one invaginating (a, b) and a few superficial contacts (a, in 6–8 μm focal planes) (in black) between a cone pedicle and RBCs. Scale bars are 20 μm in a (left) and 5 μm in b.

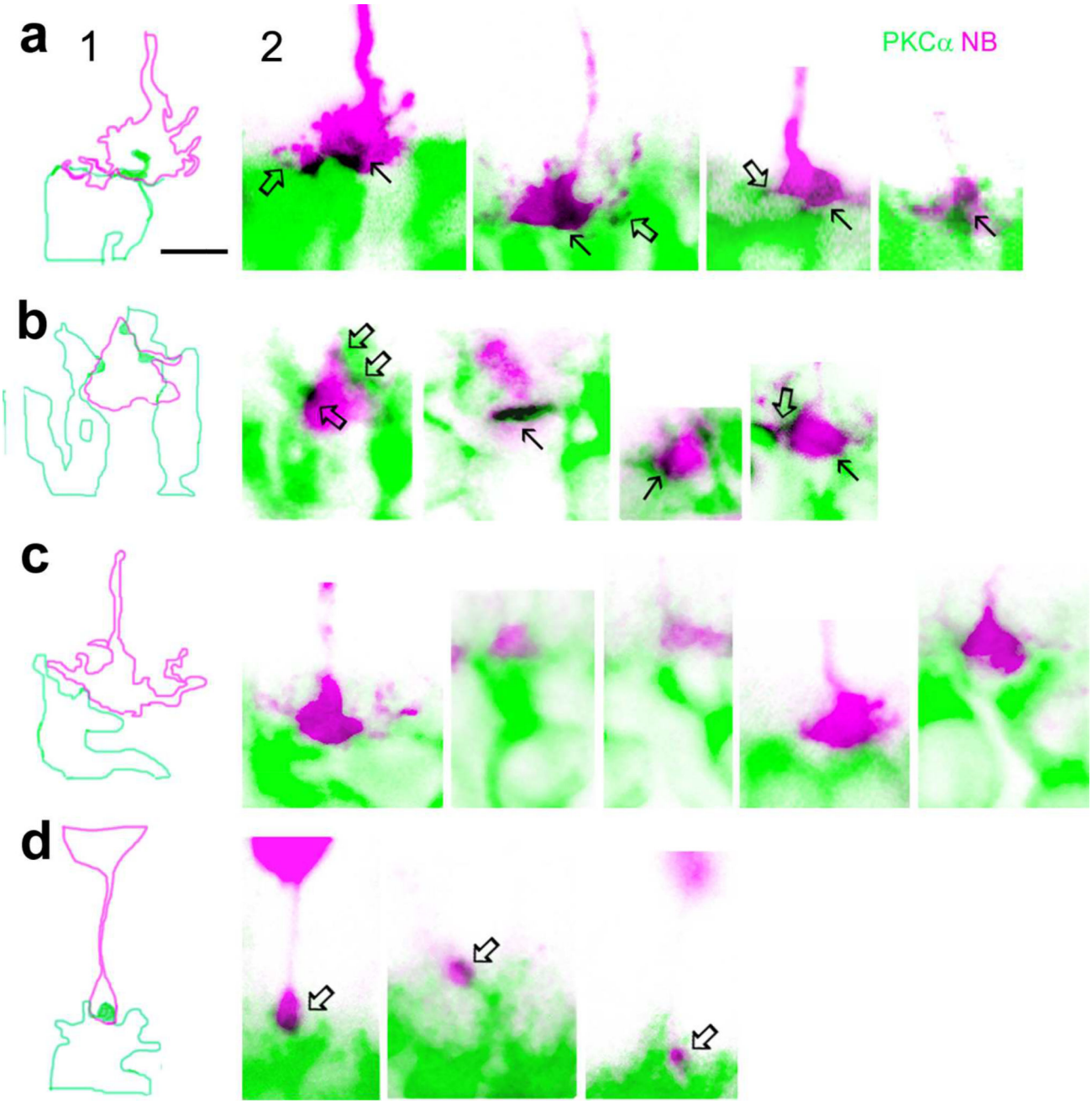

Fig. 3.

Comparison of mouse rod-RBC and cone-RBC contacts in confocal micrographs. Individual cones and rods were filled with NB and retinas were further labeled for PKCα. Images in panel 1 show outlines of RBC dendrites (green) and cone pedicles (pink) in the first image of panel 2 obtained by tracing the profiles with Photoshop software. a and b show invaginating cone-RBC contacts (in black, see arrows) where a RBC dendrite plugs deeply into the basal membrane of cone pedicles, as well as a few superficial cone-RBC putative synapses where RBC dendrites contact cone telodendrites and RBC dendritic spines bulge into the surface of cone pedicles (open arrows). c displays cone pedicles and adjacent RBC

dendrites without forming synapses. d depicts rod-RBC invaginating synapses, where a single RBC dendritic spine inserts into the center of a small rod spherule (arrows). The scale bars are 5 μm.

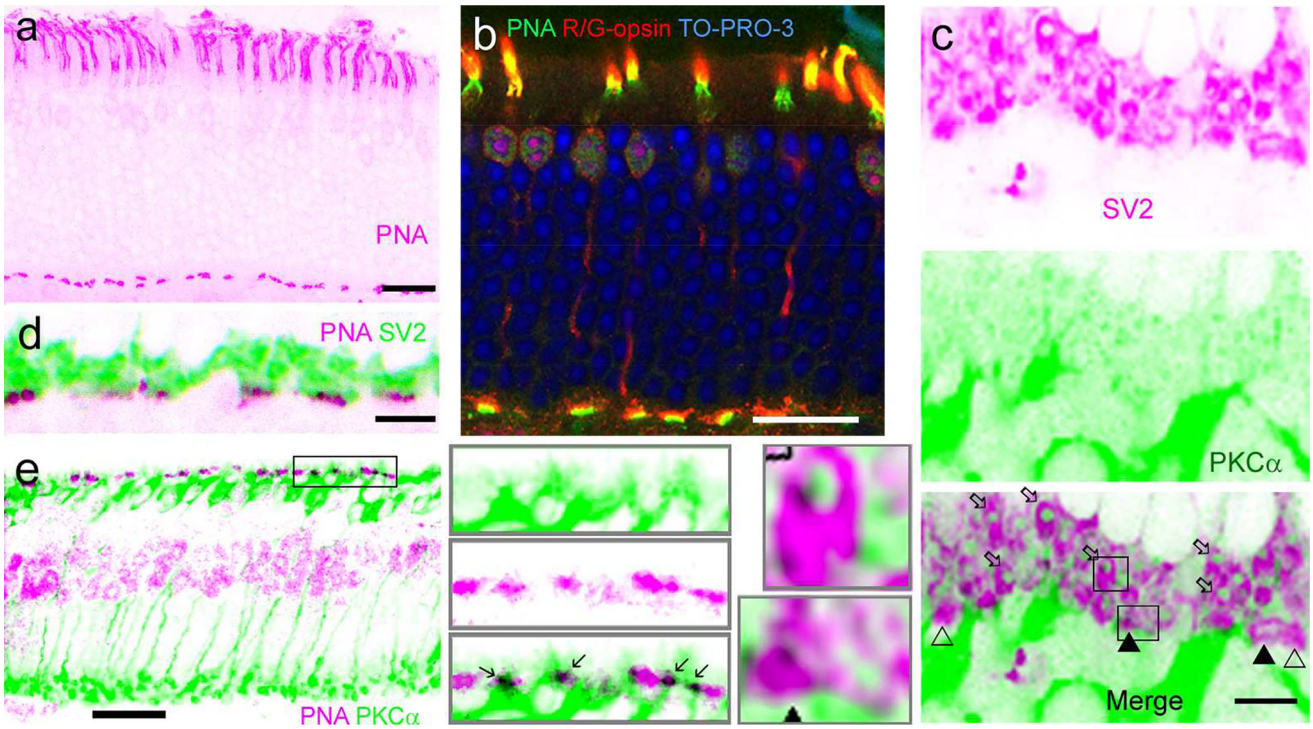

Fig. 4.

Identification of mouse cone-RBC synapses. PNA brightly labels the inner segment (a, b) and the basal membrane of cone pedicles, and cones are labeled for R/G-opsin (b). Nuclei in the outer nuclear layer (ONL) are labeled by nuclear dye TO-PRO-3 (b). Cone somas are mostly located in the first row of somas in the ONL. Cone synapses at the basal membrane, where PNA (b) and SV2 (c, d) coincide, are closer to RBC layer than all other synapses identified by SV2 in the OPL. Some PKCα-labeled RBC dendrites are colocalized with PNA in cone basal membranes (in black, in e and insets). In retinas labeled for SV2 (c and insets), rod spherules are identifiable by their strong SV2-immunoreactivity, smaller size, oval shape and more distal location (open arrows), while cone pedicles are recognizable by their triangular shape, larger size and more proximal location (triangles). Many Rod-RBC contacts are formed by a solitary RBC dendrite invaginating to the center of each rod spherule, appearing like pomegranate arils (c, bottom). Some cone pedicles receive RBC invaginating contacts (closed triangles) and some don't (open triangles) (c). Scale bars are 20 μm.

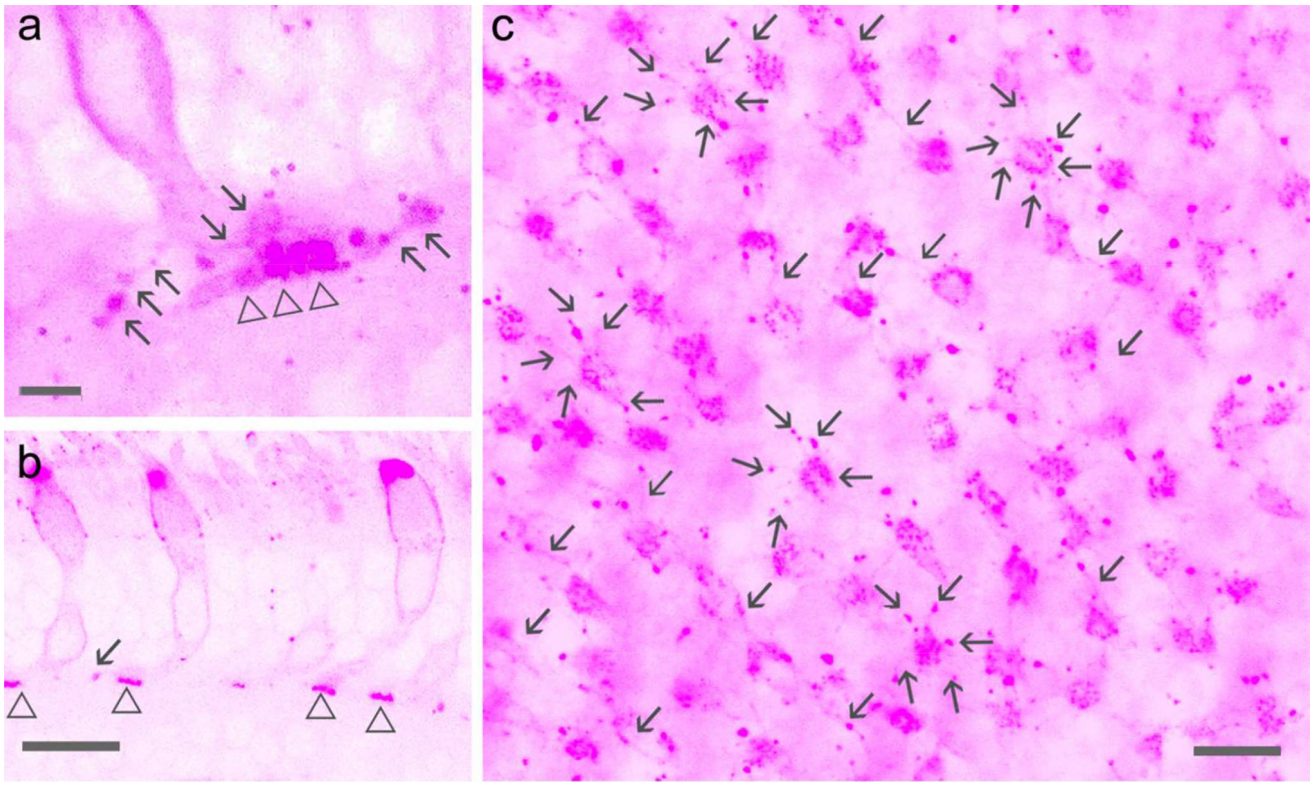

Figure 5.

Baboon cone pedicles and telodendrites labeled for PNA. Confocal micrographs show PNA-labeled cones (pink) in retinal slices (a, b) and flat-mounts (c). a and c are overexposed images. PNA signals appear as puncta in cone pedicles (triangle) and endings of cone telodendrites (arrow). Each cone pedicle sends out ~6 telodendrites. Sale bars are 1.5 μm in a and 20 μm in b and c

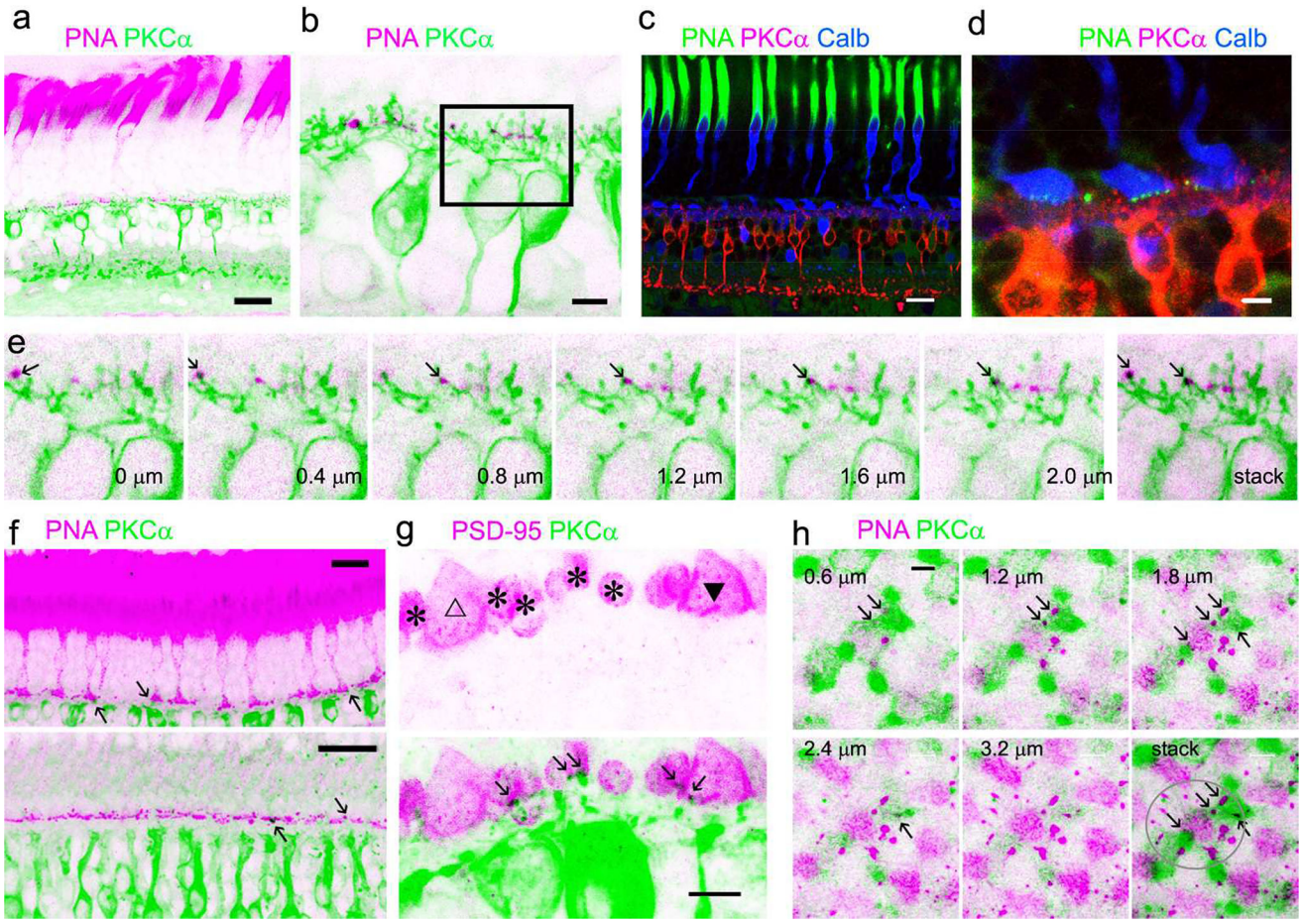

Fig. 6.

Baboon cone-RBC synapses. Retina preparations are triple- (a to d) or double-labeled. Cone somas and pedicles are brightly labeled for calbindin D-28k (Calb) (c, d). PNA intensively labels cone inner segments (a, c, e) and reveals clusters of puncta in the basal membrane of cone pedicles (d). Each cluster of PNA-positive puncta belongs to a cone pedicle (d). Consecutive confocal optical sections of a rectangular region in b show that some PKCα-labeled RBC dendrites colocalize with PNA (e). Some RBC dendrites coincide with PNA in cone pedicles (see arrows) in retinal slices (f, upper-peripheral retina, lower-para-central retina) and cone telodendrites in the flat-mount retina (h). h displays overexposed images of consecutive horizontal confocal optical sections of a cone pedicle and its telodendrites (in the circle). In retinal slices (g) large triangular cone pedicles are positively labeled for PSD95 (triangle) and distinguishable from small oval-shaped rod spherules (asterisks). RBC dendrites contact rod spherules and one cone pedicle (closed triangle) but do not contact the other cone pedicle (open triangle). Scale bars are 20 μm in a, c and f and 5 μm in the rest images.

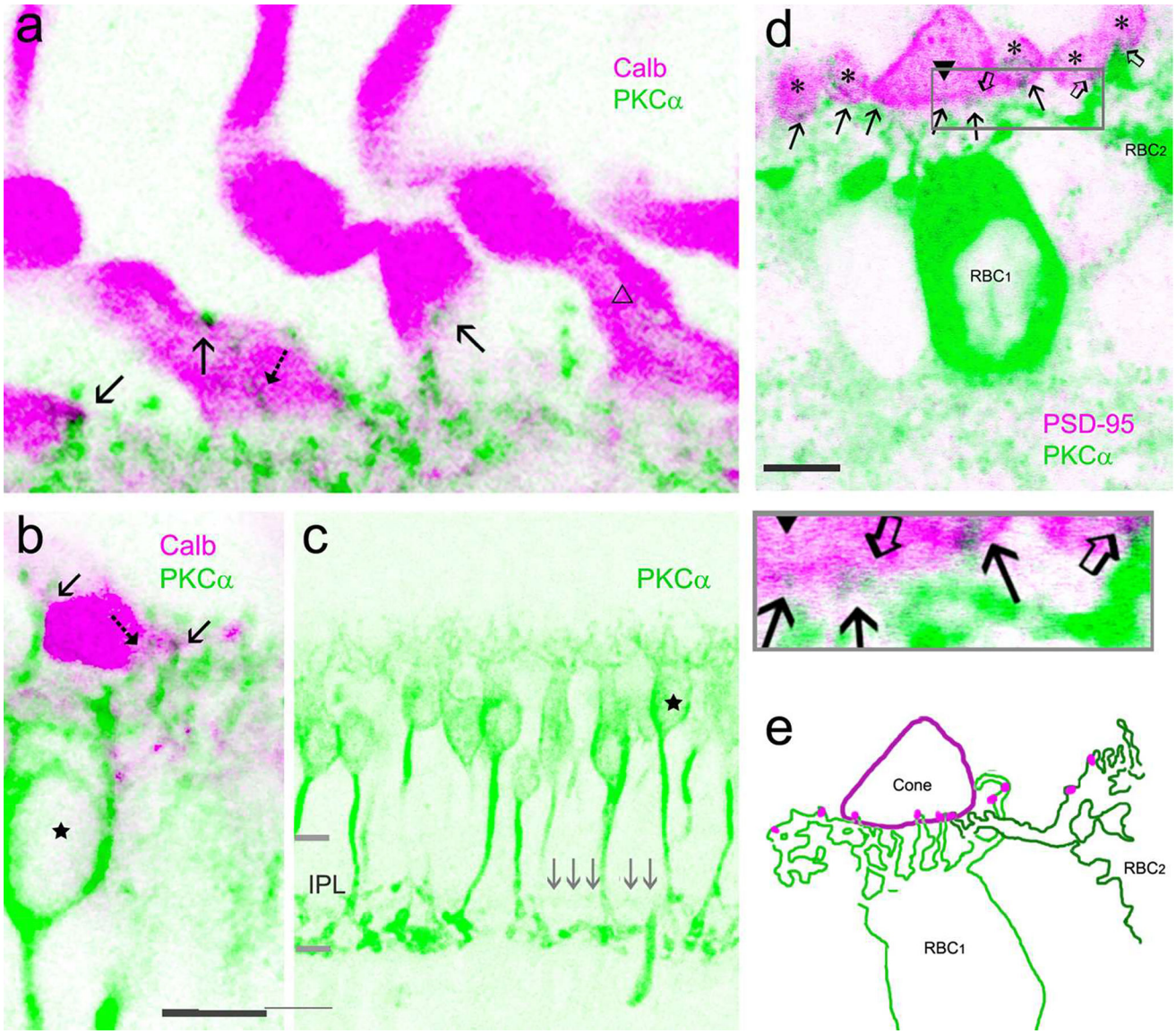

Fig. 7.

Confocal microscopy of baboon cone-RBC contacts. In a to b, cones are positively labeled by calbindin D-28k (Calb, pink). Each cone shows a tall fat sock-like pedicle with two vertically arranged segments. PKCα-labeled RBC dendrites (green) contact the lower segment, mostly by superficial contacts (arrow) and sometimes by invaginating contact (dashed arrow). Some cone pedicles do not contact RBCs (open triangle, a). The axon of the RBC (star, b and c), like those of other RBCs, branches at ~50–70% of the IPL depth and terminates near 100% of the IPL depth. The signals (gray arrows) restricted to the center of the IPL, presumably axons of DB4 cone bipolar cells, are almost invisible. In d, PKCα-labeled dendrites (green) contact both a cone pedicle (closed triangle) and rod spherules (asterisks) labeled by PSD-95 (pink), and these contacts (arrows for RBC1, open arrows for RBC2) are manually traced from the image and displayed in e (pink dots). IPL-the inner plexiform layer. The scale bar is 5 μm in a and d and 10 μm in b.

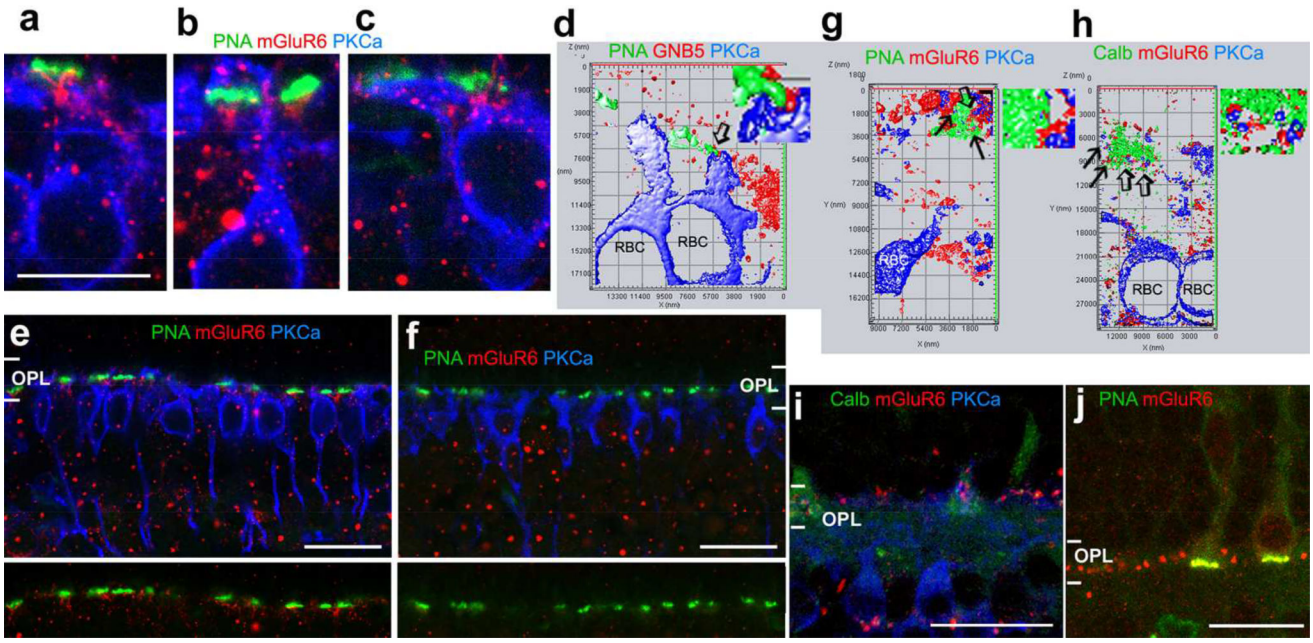

Fig. 8.

GNB5 and mGluR6 expressed in the contacts between cones and RBCs. Mouse (a–f) and baboon (g–j) retinal slices were double- or tripled-labeled. Synaptic contacts were studied in 1–2-μm-thick blocks with a resolution of 30 nm per pixel (d, g and h) and in series of optical sections ≤1 μm-thick (a–c, e and f). d, g and h display the 3D surface profile reconstructed from a series of optical sections with a step of 150–180 nm. GNB5 and mGluR6 (red) are present in contacts (arrow) formed by PKCα-labeled RBC dendrites (blue) and PNA or calbindin (Calb)-labeled cone pedicles (green) (a–d, g and h). Goat anti-mGluR6 (g, h and i) and rabbit anti-mGluR6 (the rest images) label primarily the outer plexiform layer (OPL) in the monkey retina (g to j). In the mouse retina, they label the OPL and inner nuclear layer (e), but the immunoreactivity in the OPL is absent in the mGluR6 knockout mouse (f). The distribution of GNB5 immunoreactivity in the OPL is like mGluR6 immunoreactivity (d). Small regions pointed by open arrows in d, g and h are amplified and depicted to the right. GNB5-G protein beta 5. The scale bar is 10 μm for a–c and 20 μm for e, f, i and j.

Table

Antigen	Antigen Structure	Manufacture, Product number, Dilution, Host and Clone	Reference
PKCα	Synthetic peptide corresponding to amino acids (aa.) 659–672 from the C-terminal variable (V5) region of rat PKC α conjugated to KLH	Sigma, P4334, 1: 1000, Rabbit, Polyclonal RRID: AB_477345	(Elshatory et al., 2007; Pang et al., 2013)
PKCα	Human PKCα aa. 270–427 Recombinant Protein	BD transduction, 610107, Clone 3/ PKCα (RUO), 1: 200, Mouse, Monoclonal RRID: AB_397513	(Elshatory et al., 2007; Pang et al., 2013)
Calbindin D-28k	Recombinant rat calbindin D-28k (CB) protein	Swant, CB38, 1: 1000, Rabbit, Polyclonal RRID: AB_10000340	(Fischer et al., 2008; Zhang et al., 2003)
Calbindin D-28k	Bovine kidney calbindin-D	Sigma, C9848, clone CB955, 1: 200, Mouse, Monoclonal RRID: AB_476894	(Fischer et al., 2008; Zhang et al., 2003)
PSD-95	Recombinant protein corresponding to human PSD95	Millipore, MABN68, clone K28/43, 1: 100, Mouse, Monoclonal RRID: AB_10807979	(Ivanova et al., 2013; Fischer et al., 2008)
GNB5	GNB5 (NP_057278, aa. 1–91) partial recombinant protein with GST tag.	Sigma, WH0010681M1, clone 3A3, 1: 250, Mouse Monoclonal RRID: AB_1841816	(Mojumder et al., 2009; Morgans et al., 2007)
mGluR6	A peptide mapping within a C-terminal extracellular domain of mGluR-6 of human origin.	Santa Cruz, sc-47149, 1: 1000, Goat, Polyclonal RRID: AB_784501	(Yao et al., 2005)
mGluR6	AAPPQNENAEDAK	Neuromics, RA-13105, 1: 1000, Rabbit, Polyclonal RRID: AB_2650488	(Gregg et al., 2007; Oh et al., 2007)
SV2	Purified synaptic vesicles from Ommata	DSHB, 62602, 1: 10, Mouse, Monoclonal RRID: AB_2315387	(Fischer et al., 2008; Bejarano-Escobar et al., 2012)